A scaled wave finite element method for computing scalar wave radiation and scattering in exterior domains

Denis Duhamel

A scaled wave finite element method for computing scalar wave radiation and scattering in exterior domains

Denis Duhamel

Laboratoire Navier, Ecole des Ponts, UGE/CNRS
6 et 8 Avenue Blaise Pascal,
Cité Descartes, Champs sur Marne,
77455 Marne la Vallée, cedex 2, France
Tel: + 33 1 64 15 37 28
Fax: + 33 1 64 15 37 41
email : denis.duhamel@enpc.fr

Revised version

Number of pages : 30
Number of figures : 16

Abstract

The calculation of high-frequency wave radiation in exterior domains by finite element methods can lead to large computations. In this paper, it is shown that the solution in the exterior domain can be decomposed as a series expansion of functions with an analytical part made from the product of harmonic waves and polynomials in a scaled variable and a numerical part made of a finite element approximation vectors. The solution of the radiation or scattering problem can be found by solving a sparse linear system which is set from the dynamic stiffness matrices of several scaled layers around the radiating body. These dynamic stiffness matrices are classical finite element matrices obtained from any finite element software. Moreover, accurate results can be obtained from a small number of terms in the series expansion. Several examples are given to estimate the efficiency of the proposed method.

Key words: Finite element, scaled domain, wave, Helmholtz equation, radiation, scattering, infinite domain.

1 Introduction

Many approaches have been used in the past for computing the solutions of wave problems in unbounded media. Classical methods include the boundary element method described in numerous classical textbooks like [1–5] and the fast multipole method developed by many authors like [6–9]. One can also find, for instance, the Dirichlet to Neumann (DtN) mapping proposed by [10,11] which is also quite accurate but lead to non-local boundary conditions as for the boundary element method and full matrices on the boundary. Local methods, on the contrary, are more computationaly efficient as in these methods, the condition at a border node involves only a limited number of neighbouring nodes. Various classes of local absorbent boundary conditions were for instance developed long ago by [12]. Infinite elements made with elements extending at infinity and satisfying the Sommerfeld radiation condition were proposed by [13–18]. Other absorbing boundary conditions involving differential operators of different orders on the boundary were proposed by different authors [19–22] and then improved by Bayliss and Turkel [23,24] using sequences of local non-reflecting boundary conditions and modified by [25,26]. However, all these conditions are difficult to implement above the second order because of the high order derivatives involved in their formulations. Another possibility is the addition of variables on the exterior surface as in [27–29]. They involve only second order derivatives of the auxiliary variables and so can be efficiently implemented. One can also surround the computational domain by absorbing layers, as proposed by [30,31] in the perfectly matched layer, in which the wave equation is analytically continued into complex coordinates. With a correct choice of the size of the layer and the parameters of the absorbing layer, very efficient absorptions of waves can be obtained. More details on these methods are given in [32] and a review on the different numerical methods for short wave scattering can be found in [33]. In all these local methods, a significant part of the exterior domain is meshed, and more or less accurate boundary conditions are put at the external surface of the mesh. Little or no information is given on the solution outside the meshed domain.

Among all the methods, we must especially notice the scaled boundary finite-element method proposed by [34–37]. It is based on a coordinate transform with a radial coordinate interpreted as a scaling factor with a reference to a center inside the bounded domain. The problem is formulated as a differential equation in the radial coordinate and can be solved analytically along this coordinate. The method was further developed by its authors in [38–41]. The solution is obtained by solving an eigenvalue problem from matrices built on the boundary. In case of dynamic problems, it also needs expansions in the scaled variables. These points were developed in [42,43]. This subject is still active as evidenced by recent papers [44–47]. The advantage of this method is that it gives analytical solutions in the scaled variable. Note that it can

be easily coupled with FEM models of other fluid or structural domains as shown in [48]. However, it needs special matrices defined on the boundary of the radiating body which are not the usual matrices obtained by classical finite element software.

Other interesting methods were developed for the analysis of waveguides. For example, the semi-analytical finite element (SAFE) method proposed by [49–51] and further developed by [52–57] separate the solution into an analytical harmonic function e^{ikx} into the direction of the waveguide and a finite element approximation in the cross-section. This can only be applied to uniform waveguides and needs special matrices defined on the cross-section of the waveguide. So the approach has some common points with the scaled boundary finite-element method: an analytical expression of the solution in radial/waveguide direction and special matrices in the boundary/cross-section. This method has been applied to various problems and some recent developments were proposed, for instance, by [58–60].

For non uniform waveguides with truly periodic structures, the Wave Finite Element (WFE) method can be used. This consists in computing wave modes (propagation constants, wave shapes) of a periodic structure from the finite element (FE) model of a substructure and its related mass, damping and stiffness matrices which can be obtained from any FE software. Afterwards, these wave modes can be used to calculate the harmonic response of periodic structures in an efficient way, i.e., by computing small matrix systems for one substructure, or a few of them. The main steps of the method can be found in [61–64]. Also, some of its recent extensions and applications are reported in [65–74]. Compared to the SAFE method, the WFE can deal with more general structures and do not need the development of special matrices but can use matrices produced by commercial FE software. This Floquet's theory was applied to exterior problems by [75,76] by dividing the exterior domain into layers and trying to apply the WFE on them with possible corrections on the solution to obtain constant energy flux through the layers. However, as the matrices in the different layers of the exterior domain are not constant, only approximate solutions have been obtained.

In this paper, we propose to improve these last attempts of [75,76] by coupling the equilibrium equations between adjacent layers as in the WFE approach and which only needs classical finite element matrices, to the expansion of the solution suggested by the scaled boundary finite element. The solution in the exterior domain will be decomposed as a sum of elementary functions made of harmonic waves multiplied by polynomials and finite element approximation vectors. The solution can then be found by solving a sparse linear system which is set from the dynamic stiffness matrices of several scaled layers around the radiating body. These dynamic stiffness matrices are classical finite element matrices obtained from any finite element software, so eliminating the need

of building special matrices. Accurate results can be obtained from a small number of terms in the series expansion. So a description of the solution in the exterior domain can be found for general geometries. The paper is divided into three sections and is outlined as follows. In the second section, the principles of the method are described in general. In the third section, examples are described to get a clear insight in the proposed approach before concluding remarks.

2 Solution in the exterior domain

2.1 Behaviour of a layer

We consider the general case of a convex body Ω surrounded by an infinite domain as in figure 1. To simplify, we consider here two-dimensional problems only. Linear waves are supposed to propagate in this exterior domain. They are described by the Helmholtz equation

$$\Delta q + k^2 q = 0 \tag{1}$$

with $k = \omega/c$ the wavenumber, ω the circular frequency and c the velocity. Boundary conditions are applied on the boundary surface S_0 and at infinity such that

$$\begin{aligned} q &= q_0 \quad on \ S_0^D \\ \frac{\partial q}{\partial n} &= r_0 \quad on \ S_0^N \\ \frac{\partial q}{\partial n} - ikq &= o(\frac{1}{\sqrt{r}}) \quad for \ r \to \infty \end{aligned} \tag{2}$$

with S_0^D and S_0^N the parts of S_0 where respectively the Dirichlet and Neumann boundary conditions are applied and q_0 and r_0 given functions on S_0. The last relation is the Sommerfeld radiation condition for two-dimensional problems.

A layer n, defined as the domain Ω_n between surfaces S_n and S_{n+1}, is described by a finite element model. The surface S_n is defined by a constant value of the scaled parameter $\xi = \xi_n$ with $\xi_n = 1 + \sum_{i=0}^{i=n-1} \mathrm{d_i}$ (as in the scaled boundary element method) where the $\mathrm{d_i}$ are the variables giving the thickness in term of ξ of each layer and $\xi = \xi_0$ with $\xi_0 = 1$ defines the surface S_0 of the radiating body. A layer can be meshed with an arbitrary number of elements using the full possibilities of usual finite element software. This makes it possible to process structures of complex shapes directly from their dynamic

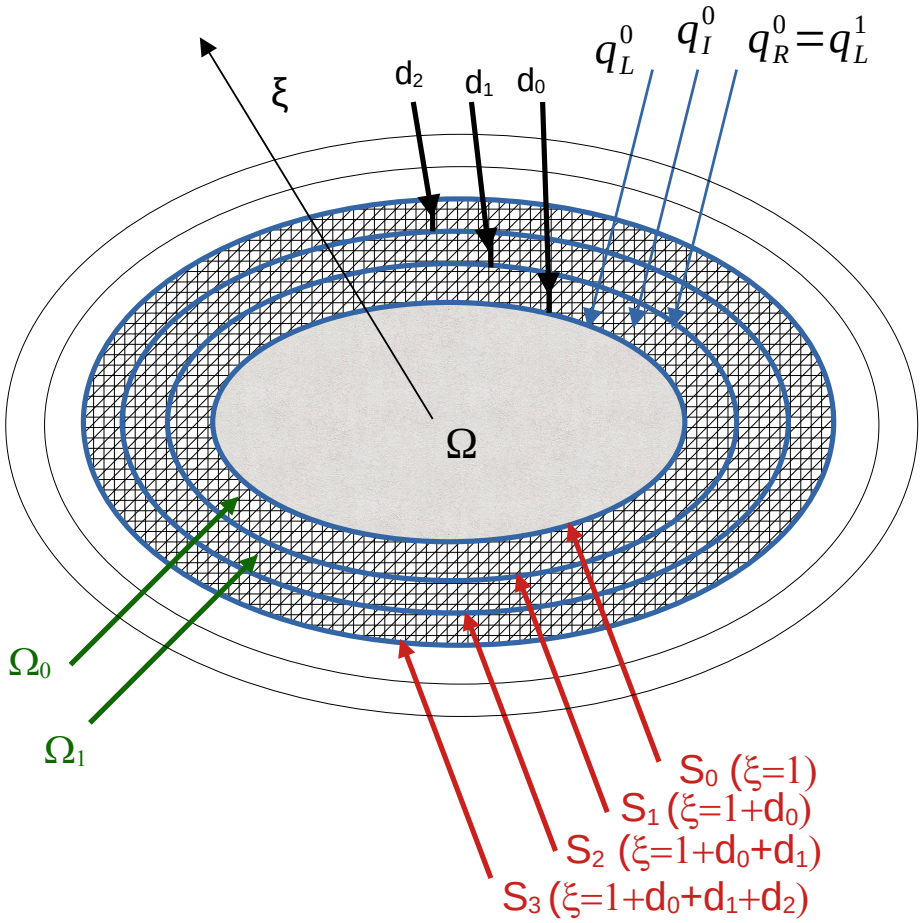

Fig. 1. Exterior domain divided into different layers.

stiffness matrix without having to go into the details of the implementation of the finite elements (shape functions, order of the elements, integration techniques, ...) and to be able to potentially generalize the proposed method to other situations without substantial modification of the software. The discrete dynamic behaviour of a layer n obtained from a finite element model at a circular frequency ω is thus given by

$$(\mathbf{K}^n - \omega^2 \mathbf{M}^n)\mathbf{q}^n = \mathbf{f}^n \tag{3}$$

where $\mathbf{K}^n$ and $\mathbf{M}^n$ are the stiffness and mass matrices respectively, $\mathbf{f}^n$ is the vector of internal forces and $\mathbf{q}^n$ the vector of the degrees of freedom. Introducing the dynamic stiffness matrix of the layer $\mathbf{D}^n = \mathbf{K}^n - \omega^2 \mathbf{M}^n$, decomposing into degrees of freedom of the left boundary (L) associated to the dofs in S_n, interior dofs (I) and right boundary dofs (R) associated to dofs in S_{n+1}, and assuming that there is no external force on the interior nodes, results in the

following relation

$$\begin{bmatrix} \mathbf{D}_{LL}^n & \mathbf{D}_{LI}^n & \mathbf{D}_{LR}^n \\ \mathbf{D}_{IL}^n & \mathbf{D}_{II}^n & \mathbf{D}_{IR}^n \\ \mathbf{D}_{RL}^n & \mathbf{D}_{RI}^n & \mathbf{D}_{RR}^n \end{bmatrix} \begin{bmatrix} \mathbf{q}_L^n \\ \mathbf{q}_I^n \\ \mathbf{q}_R^n \end{bmatrix} = \begin{bmatrix} \mathbf{f}_L^n \\ \mathbf{0} \\ \mathbf{f}_R^n \end{bmatrix} \tag{4}$$

The assumption that there is no force on the interior degrees of freedom is satisfied for free waves inside the structure for which the forces on a layer are only produced by boundary forces from the adjacent layers.

2.2 Relations between adjacent layers

At the interface between layers $n-1$ and n (on surface S_n), there is continuity of the displacement and equilibrium of the forces, so that one has

$$\mathbf{q}_L^n = \mathbf{q}_R^{n-1} \tag{5}$$
$$\mathbf{f}_L^n + \mathbf{f}_R^{n-1} = 0 \tag{6}$$

The equilibrium of the forces leads to the relation

$$\mathbf{D}_{RL}^{n-1}\mathbf{q}_L^{n-1} + \mathbf{D}_{RI}^{n-1}\mathbf{q}_I^{n-1} + \mathbf{D}_{RR}^{n-1}\mathbf{q}_R^{n-1} + \mathbf{D}_{LL}^{n}\mathbf{q}_L^{n} + \mathbf{D}_{LI}^{n}\mathbf{q}_I^{n} + \mathbf{D}_{LR}^{n}\mathbf{q}_R^{n} = 0 \tag{7}$$

or, using (5) and denoting the vector of displacement $\mathbf{q}^n$ on the surface S_n, this can be written as

$$\mathbf{D}_{RL}^{n-1}\mathbf{q}^{n-1} + \mathbf{D}_{RI}^{n-1}\mathbf{q}_I^{n-1} + (\mathbf{D}_{RR}^{n-1} + \mathbf{D}_{LL}^{n})\mathbf{q}^{n} + \mathbf{D}_{LI}^{n}\mathbf{q}_I^{n} + \mathbf{D}_{LR}^{n}\mathbf{q}^{n+1} = 0 \tag{8}$$

This must be completed by the relations for the internal degrees of freedom in domains Ω_n and Ω_{n+1}, given by

$$\mathbf{D}_{IL}^{n-1}\mathbf{q}^{n-1} + \mathbf{D}_{II}^{n-1}\mathbf{q}_I^{n-1} + \mathbf{D}_{IR}^{n-1}\mathbf{q}^{n} = \mathbf{0} \tag{9}$$
$$\mathbf{D}_{IL}^{n}\mathbf{q}^{n} + \mathbf{D}_{II}^{n}\mathbf{q}_I^{n} + \mathbf{D}_{IR}^{n}\mathbf{q}^{n+1} = \mathbf{0} \tag{10}$$

So assembling relations (8), (9) and (10) yields

$$\mathbf{D}_T^n \mathbf{Q}_n = \mathbf{0} \tag{11}$$

with

$$\mathbf{D}_T^n = \begin{pmatrix} \mathbf{D}_{RL}^{n-1} & \mathbf{D}_{RI}^{n-1} & \mathbf{D}_{RR}^{n-1} + \mathbf{D}_{LL}^n & \mathbf{D}_{LI}^n & \mathbf{D}_{LR}^n \\ \mathbf{D}_{IL}^{n-1} & \mathbf{D}_{II}^{n-1} & \mathbf{D}_{IR}^{n-1} & \mathbf{0} & \mathbf{0} \\ \mathbf{0} & \mathbf{0} & \mathbf{D}_{IL}^n & \mathbf{D}_{II}^n & \mathbf{D}_{IR}^n \end{pmatrix}, \quad \mathbf{Q}_n = \begin{pmatrix} \mathbf{q}^{n-1} \\ \mathbf{q}_I^{n-1} \\ \mathbf{q}^n \\ \mathbf{q}_I^n \\ \mathbf{q}^{n+1} \end{pmatrix} \tag{12}$$

Note that in case of no interior node, this simplifies to

$$\mathbf{D}_T^n = \begin{pmatrix} \mathbf{D}_{RL}^{n-1} & \mathbf{D}_{RR}^{n-1} + \mathbf{D}_{LL}^n & \mathbf{D}_{LR}^n \end{pmatrix}, \quad \mathbf{Q}_n = \begin{pmatrix} \mathbf{q}^{n-1} \\ \mathbf{q}^n \\ \mathbf{q}^{n+1} \end{pmatrix} \tag{13}$$

Note also that $\mathbf{Q}_n$ is the vector made of the dofs associated to the domain $\Omega_{n-1} \cup \Omega_n$ and, if we denote by M_n this number of dofs, the size of $\mathbf{Q}_n$ is $M_n \times 1$ while the number of lines of $\mathbf{D}_T^n$ equals the number of dofs on the surface S_n plus the number of internal degrees of freedom in $\Omega_{n-1} \cup \Omega_n$, the whole which is denoted m_n, and so the size of $\mathbf{D}_T^n$ is $m_m \times M_n$ with $m_m < M_n$.

2.3 Series expansion of the solution

As we deal with two-dimensional problems, we expect a large distance behaviour like $\frac{e^{ikr}}{\sqrt{r}}$. So the displacement at a node of location $\mathbf{r}_j$ of scaled parameter ξ_j will be assumed given by the expansion,

$$q(\mathbf{r}_j) = \sum_{p=0}^{p=P} \left(a_{jp} \xi_j^{-(2p+1)/2} \right) e^{ik|\mathbf{r}_j|} \tag{14}$$

in term of parameters a_{jp} to be found. Note that this expansion includes both the distance r_j of the node j to the center of the object and the parameter ξ_j which locates the surface to which the node j belongs. For a node j_s on the surface of the object, we therefore have $\xi_{j_s} = 1$ and the expansion reduces to

$$q(\mathbf{r}_{j_s}) = \left(\sum_{p=0}^{p=P} a_{j_s p} \right) e^{ik|\mathbf{r}_{j_s}|} \tag{15}$$

The form of the expansion (14) was suggested by the expansion of Hankel's functions for large arguments. Other expansion choices are probably possible. Note also that we make the assumption that the domains are meshed in an

identical way up to the scaled parameter ξ, see figure 2. So the nodes on the different surfaces S_n are located on the same radial lines and the nodes on a surface S_n can be obtained from the nodes on the surface S_{n-1} by scaling in ξ. So the value of $q(\mathbf{r}_j)$ is expressed in term of $p+1$ parameters a_{jp} with

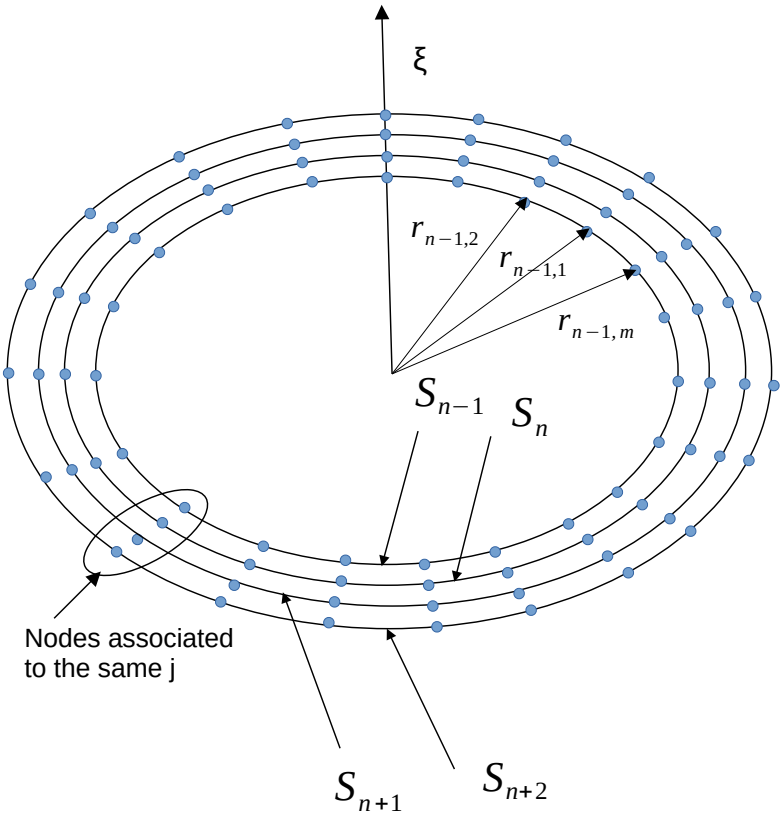

Fig. 2. Mesh of the surfaces S_n.

$0 \leq p \leq P$ associated to the same direction on different surfaces and so for a fixed value of j which defines the radial direction to which $\mathbf{r}_j$ belongs. The vector of displacement $\mathbf{Q}_n$ of the dofs of the domain $\Omega_{n-1} \cup \Omega_n$ can thus be written as

$$\mathbf{Q}_n = \begin{pmatrix} \mathbf{T}_a^n & \mathbf{T}_I^n \end{pmatrix} \begin{pmatrix} \mathbf{a} \\ \mathbf{q}_I \end{pmatrix} = \mathbf{T}^n \begin{pmatrix} \mathbf{a} \\ \mathbf{q}_I \end{pmatrix} \tag{16}$$

with $\mathbf{T}^n = \begin{pmatrix} \mathbf{T}_a^n & \mathbf{T}_I^n \end{pmatrix}$ and where the vector of the parameters a_{jp} is

$$\mathbf{a} = \begin{pmatrix} \mathbf{a}_0 \\ \vdots \\ \mathbf{a}_p \\ \vdots \\ \mathbf{a}_P \end{pmatrix}, \quad with \quad \mathbf{a}_p = \begin{pmatrix} a_{1p} \\ \vdots \\ a_{mp} \end{pmatrix} \tag{17}$$

and

$$\mathbf{T}_a^n = \left(\mathbf{t}_n, \mathbf{\Xi}_n.\mathbf{t}_n, \ldots, \mathbf{\Xi}_n^P.\mathbf{t}_n \right) \tag{18}$$

with

$$\mathbf{t}_n = \left(\xi_{n,j}^{-1/2} e^{ik|\mathbf{r}_{n,j}|} \, \mathrm{d}_{jj'} \right)_{j=1...M, j'=1...m} \tag{19}$$

$$\mathbf{\Xi}_n = diag(\frac{1}{\xi_{n,j}})_{j=1...M} \tag{20}$$

with *diag* meaning a diagonal matrix and the domain $\Omega_{n-1} \cup \Omega_n$ is supposed meshed with M nodes of positions $\mathbf{r}_{n,j}$ for $j = 1...M$ with the associated scaled parameters $\xi_{n,j}$ and m is the number of nodes on a surface S_n. Note that the $\xi_j^{-(2p+1)/2}$ factor can be found for the $\xi_j^{-1/2}$ part in the vector $\mathbf{t}_n$ and for the ξ_j^{-p} part in the matrix $\mathbf{\Xi}_n^p$. The parameter $d_{jj'}$ equals 1 if the node number j in domain $\Omega_{n-1} \cup \Omega_n$ is not an interior node and if node j is associated to node j' on surface S_n in the way shown in figure 2. In other words, nodes on the same radial line are associated to the same j'. So the matrix $\mathbf{t}_n$ is sparse and has only one non zero element on each line. The vector $\mathbf{q}_I$ is the global vector of interior degrees of freedom associated to the considered domains. The matrix $\mathbf{T}_I^n$ is a matrix made of zeros and ones which extracts the subvectors $\mathbf{q}_I^{n-1}$ and $\mathbf{q}_I^n$ of relation (12) from $\mathbf{q}_I$.

Combining with relation (11), the equation for the layer can be finally written as

$$\mathbf{S}^n \begin{pmatrix} \mathbf{a} \\ \mathbf{q}_I \end{pmatrix} = (\mathbf{D}_T^n \mathbf{T}^n) \begin{pmatrix} \mathbf{a} \\ \mathbf{q}_I \end{pmatrix} = \mathbf{0} \tag{21}$$

where the precedent relation defines the matrix $\mathbf{S}^n$. The number of equations equals m_n, the number of dofs on the surface S_n plus the number of interior dofs in $\Omega_{n-1} \cup \Omega_n$. Note that according to the shape of the matrix $\mathbf{T}^n$ seen in relations (16) and (18), the matrix $\mathbf{S}^n$ is given by

$$\mathbf{S}^n = \left(\mathbf{D}_T^n \mathbf{t}_n, \mathbf{D}_T^n \mathbf{\Xi}_n.\mathbf{t}_n, \ldots, \mathbf{D}_T^n \mathbf{\Xi}_n^P.\mathbf{t}_n, \mathbf{D}_T^n.\mathbf{T}_I^n \right) \tag{22}$$

and is also a sparse matrix as $\mathbf{D}_T^n$, which is sparse, multiplies only other sparse matrices.

2.4 Global solution

Now, relations (16) and (21) are applied for the surface S_0 and layers $n_1, n_2, ..., n_P$, see Figure 1. We consider first a Dirichlet problem with the given displacement $\mathbf{q}_0$ on the boundary surface S_0. Using relation (16) leads to

$$\mathbf{q}_0 = \mathbf{T}_r^0 \begin{pmatrix} \mathbf{a} \\ \mathbf{q}_I \end{pmatrix} \tag{23}$$

with $\mathbf{T}_r^0$ obtained in the same way as (16) but keeping only the lines associated to the dofs of the surface S_0. This is also the component $\mathbf{q}_0$ of vector $\mathbf{Q}_1$ in relations (12) and (16). So, the number of equations equals the number of dofs on surface S_0, denoted m.

Then, we choose P central layers $n_1, ..., n_P$, and around each layer we apply the relation (21) so that for the other layers n_i, the relation is

$$\mathbf{S}^{n_i} \begin{pmatrix} \mathbf{a} \\ \mathbf{q}_I \end{pmatrix} = 0 \tag{24}$$

Assembling relations (23) and (24), finally, the global system to solve is

$$\begin{pmatrix} \mathbf{T}_r^0 \\ \mathbf{S}^{n_1} \\ \vdots \\ \mathbf{S}^{n_P} \end{pmatrix} \begin{pmatrix} \mathbf{a} \\ \mathbf{q}_I \end{pmatrix} = \begin{pmatrix} \mathbf{q}_0 \\ \mathbf{0} \\ \vdots \\ \mathbf{0} \end{pmatrix} \tag{25}$$

The solution of this system gives the parameters a_{jp} and the solution for any node can be obtained by the expansion (14) and the components of $\mathbf{q}_I$. To obtain a square system a parameter a_{jp} must be associated to each dof of S_{n_i} and to each dof of S_0.

In case of a Neumann problem where the external force $\mathbf{f}_0$ is given on surface S_0, relation (23) is changed to

$$\begin{pmatrix} \mathbf{f}_0 \\ \mathbf{0} \end{pmatrix} = \mathbf{S}_r^0 \begin{pmatrix} \mathbf{a} \\ \mathbf{q}_I \end{pmatrix} \tag{26}$$

with

$$\mathbf{S}_r^0 \begin{pmatrix} \mathbf{a} \\ \mathbf{q}_I \end{pmatrix} = \mathbf{D}_L^0 \mathbf{T}_0^1 \begin{pmatrix} \mathbf{a} \\ \mathbf{q}_I \end{pmatrix} \tag{27}$$

with $\mathbf{D}_L^0$ the submatrix of $\mathbf{D}^0$ with only the lines associated to the dofs of S_0 and the interior dofs of Ω_0 (first and second lines of relation (4)) and $\mathbf{T}_0^1$ the submatix of $\mathbf{T}^1$ with only the lines associated to the dofs of Ω_0 (first three lines of $\mathbf{Q}_1$ in relation (12) and (16)). The right member of relation (25) is changed so that the final relation is now

$$\begin{pmatrix} \mathbf{S}_r^0 \\ \mathbf{S}^{n_1} \\ \vdots \\ \mathbf{S}^{n_P} \end{pmatrix} \begin{pmatrix} \mathbf{a} \\ \mathbf{q}_I \end{pmatrix} = \begin{pmatrix} \mathbf{f}^0 \\ \mathbf{0} \\ \vdots \\ \mathbf{0} \end{pmatrix} \tag{28}$$

The number of equations in relation (25) equals $m + P(m + 2n_{int})$ and in (28) it equals $m + n_{int} + P(m + 2n_{int})$ with n_{int} the number of interior dofs in a domain. Note that the linear system to solve is sparse.

2.5 Coupling with another FEM domain

The expansion (14) is efficient for large enough frequencies and for convex domains. We consider here the more general case of radiation by a body of any shape as in the figure 3. Note that here the radiating body is non-convex and therefore the previous method cannot be applied directly. So, we divide the domain outside the radiating body into two subdomains. The first subdomain is inside a convex surface noted S_0 and is described by a dynamic stiffness matrix of a classical finite element model obtained by any finite element software (the grid part in the figure). The second subdomain outside the surface S_0 can be described by the model presented previously since the surface S_0 is convex. We will then specify the equations satisfied in each of the two subdomains and the global relation obtained by coupling the two subdomains. The domain interior to the surface S_0 which is described by a classical finite element model satisfied the following relation.

$$\begin{bmatrix} \mathbf{D}_{bb} & \mathbf{D}_{bi} & \mathbf{D}_{b0} \\ \mathbf{D}_{ib} & \mathbf{D}_{ii} & \mathbf{D}_{i0} \\ \mathbf{D}_{0b} & \mathbf{D}_{0i} & \mathbf{D}_{00} \end{bmatrix} \begin{bmatrix} \mathbf{q}_b \\ \mathbf{q}_i \\ \mathbf{q}_0 \end{bmatrix} = \begin{bmatrix} \mathbf{f}_b \\ \mathbf{0} \\ \mathbf{f}_0 \end{bmatrix} \tag{29}$$

with the subscript b describing the dofs belonging to the surface S_b where the boundary conditions are prescribed (the surface of the radiating body), 0 the dofs belonging to the coupling interface S_0 between the domain described by classical FEM and the exterior domain described by the expansion (14) and i the dofs internal to the FEM domain, see figure 3.

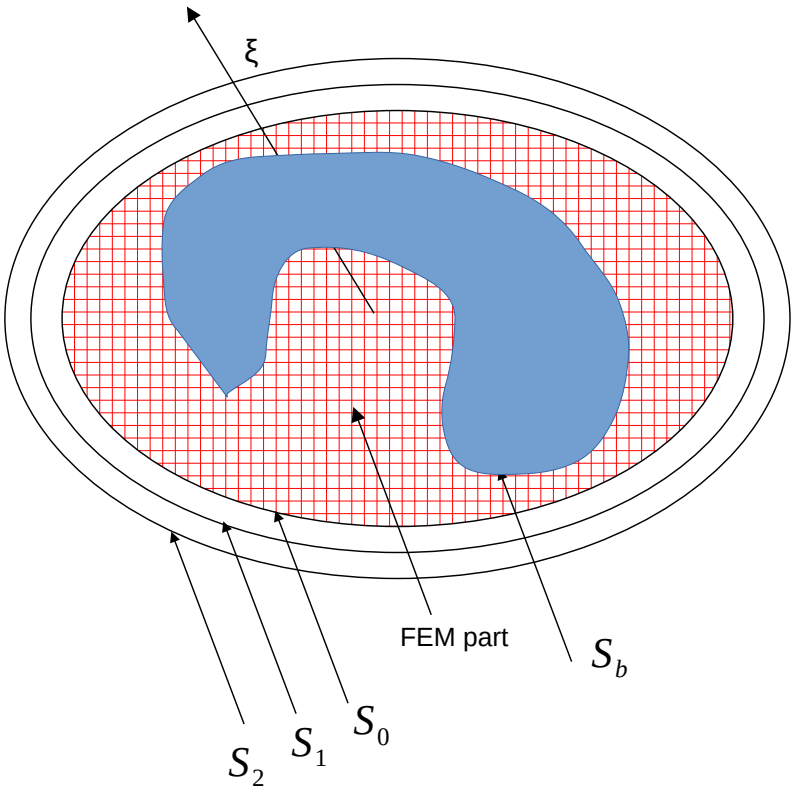

Fig. 3. Case of a non convex domain.

On the surface S_0, one has the relations (23) and (26) so that

$$\mathbf{q}^0 = \mathbf{T}_r^0 \begin{pmatrix} \mathbf{a} \\ \mathbf{q}_I \end{pmatrix} \tag{30}$$

$$\begin{pmatrix} \mathbf{f}_0 \\ \mathbf{0} \end{pmatrix} = \mathbf{S}_r^0 \begin{pmatrix} \mathbf{a} \\ \mathbf{q}_I \end{pmatrix} = \begin{pmatrix} \mathbf{S}_{r0}^0 \\ \mathbf{S}_{ri}^0 \end{pmatrix} \begin{pmatrix} \mathbf{a} \\ \mathbf{q}_I \end{pmatrix} \tag{31}$$

with the second line of (31) associated to the interior dofs of Ω_0. Assembling relations (29), (30), (31) with the relations (21) for the other external surfaces

leads to

$$\begin{bmatrix} \mathbf{D}_{bb} & \mathbf{D}_{bi} & \mathbf{D}_{b0}\mathbf{T}_r^0 \\ \mathbf{D}_{ib} & \mathbf{D}_{ii} & \mathbf{D}_{i0}\mathbf{T}_r^0 \\ \mathbf{D}_{0b} & \mathbf{D}_{0i} & \mathbf{D}_{00}\mathbf{T}_r^0 + \mathbf{S}_{r0}^0 \\ \mathbf{0} & \mathbf{0} & \mathbf{S}_{ri}^0 \\ \mathbf{0} & \mathbf{0} & \mathbf{S}^{n_1} \\ \vdots & \vdots & \vdots \\ \mathbf{0} & \mathbf{0} & \mathbf{S}^{n_P} \end{bmatrix} \begin{bmatrix} \mathbf{q}_b \\ \mathbf{q}_i \\ \mathbf{a} \\ \mathbf{q}_I \end{bmatrix} = \begin{bmatrix} \mathbf{f}_b \\ \mathbf{0} \\ \mathbf{0} \\ \mathbf{0} \\ \mathbf{0} \\ \vdots \\ \mathbf{0} \end{bmatrix} \tag{32}$$

This system can be solved when $\mathbf{q}_b$ or $\mathbf{f}_b$ is known on the boundary S_b and the solution gives the displacement in the FEM part and the coefficients of the expansion (14).

3 Numerical examples

3.1 Two-dimensional axisymmetric example

In this first simple example, we consider an infinite membrane under harmonic excitation with normal displacement q satisfying the Helmholtz equation

$$E\Delta q + \rho\omega^2 q = 0 \tag{33}$$

The wavenumber is $k = \omega/c$ with $c = \sqrt{E/\rho}$. This is also the case of acoustic radiation with a given value of the sound velocity c. The radiating body is supposed to be a disk and we are looking for axisymmetric solutions. The radial shape functions are

$$\begin{aligned} N_1(\xi) &= \frac{1}{2}(1-\xi) \\ N_2(\xi) &= \frac{1}{2}(1+\xi) \end{aligned} \tag{34}$$

The radius is interpolated by $r(\xi) = r_1 N_1(\xi) + r_2 N_2(\xi)$ and the elements of the mass matrix for axisymmetric solutions are given by

$$
\begin{aligned}
m_{ij} &= 2\pi \int_{r_1}^{r_2} \rho N_i(r) N_j(r) r dr \\
&= \pi\rho(r_2 - r_1) \int_{-1}^{1} N_i(\xi) N_j(\xi) r(\xi) d\xi \\
\mathbf{m} &= \pi\rho(r_2 - r_1) \begin{pmatrix} \frac{r_1}{2} + \frac{r_2}{6} & \frac{r_1}{6} + \frac{r_2}{6} \\ \frac{r_1}{6} + \frac{r_2}{6} & \frac{r_1}{6} + \frac{r_2}{2} \end{pmatrix}
\end{aligned} \tag{35}
$$

The elements of the stiffness matrix are

$$
\begin{aligned}
k_{ij} &= 2\pi E \int_{r_1}^{r_2} \frac{\partial N_i(r)}{\partial r} \frac{\partial N_j(r)}{\partial r} r dr \\
&= \frac{4\pi E}{r_2 - r_1} \int_{-1}^{1} \frac{\partial N_i(\xi)}{\partial \xi} \frac{\partial N_j(\xi)}{\partial \xi} r(\xi) d\xi \\
\mathbf{k} &= \frac{\pi E(r_1 + r_2)}{(r_2 - r_1)} \begin{pmatrix} 1 & -1 \\ -1 & 1 \end{pmatrix}
\end{aligned} \tag{36}
$$

So that the dynamic stiffness matrix in the domain n is given by

$$
\mathbf{D}^n = \frac{\pi E}{d}(r_n + r_{n+1}) \begin{pmatrix} 1 & -1 \\ -1 & 1 \end{pmatrix} - \omega^2 \frac{\pi}{6} \rho d \begin{pmatrix} 3r_n + r_{n+1} & r_n + r_{n+1} \\ r_n + r_{n+1} & r_n + 3r_{n+1} \end{pmatrix} \tag{37}
$$

with r_n the radius of surface S_n. In the following, one takes $E = 1$ and everything is given in term of kr. The analytical solution for a uniform displacement q_0 at $r = r_0$ is given by

$$
q(\xi) = \frac{H_0(kr)}{H_0(kr_0)} q_0 \tag{38}
$$

with H_0 is the Hankel function of first type and order 0.

This problem was solved with the proposed method for different wavenumbers k such that $0.001 \leq kr_0 \leq 1000$. First consider the case $kr_0 = 1$ with different values of the number of polynomial coefficients given by P. The radius of surface S_n is such that $kr_n = 1 + nke$ with $ke = 0.005$ and $\xi_n = 1 + nd$ and $d = ke/max(1, kr_0)$. Figure 4 presents the real and imaginary parts of the solution in the domain $50 \leq kr \leq 60$ for different values of P. One clearly sees that $P = 0$, meaning taking only a constant for the polynomial, yields some errors. The solution is clearly improved with $P \geq 1$. The relative error defined as $\frac{|q_{num} - q_{ana}|}{|q_{ana}|}$ is plotted in figure 5. Except for low values of kr, the error is almost constant for a given value of P and the value of the error decreases as P increases. For instance, taking $P = 3$, leads to an error of less than 1%.

Now, we are interested in the influence of the wave number k on the solution of the problem. So, the solutions for different values of kr_0 are presented in figures

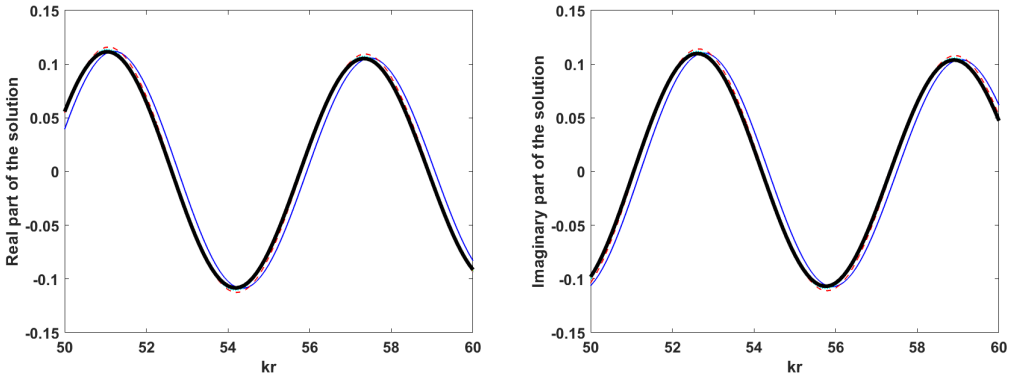

(a) Real part. (b) Imaginary part.

Fig. 4. Real part (a) and imaginary part (b) of the solution for different values of P, — P = 0, - - P = 1,. . . P = 2,-.- P = 3, ▬▬ analytical solution.

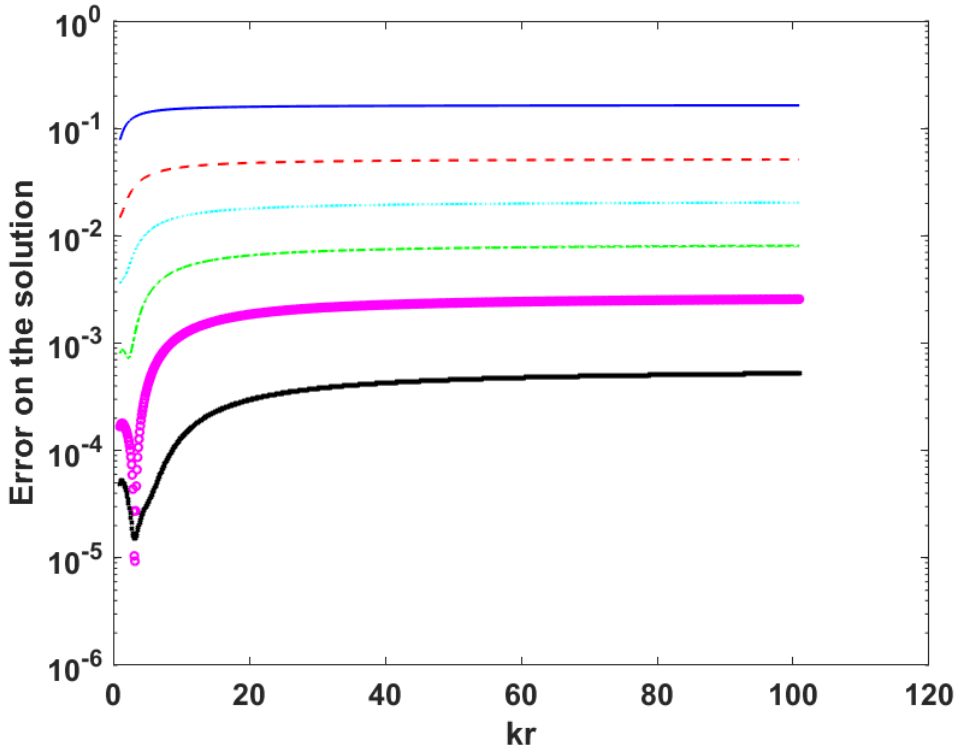

Fig. 5. Relative error on the solution for different values of P, — P = 0, - - P = 1,... P = 2,-.- P = 3, ooo P = 4, xxx P = 5.

6 and 7 in the domain $max(kr_0, 1) \leq kr \leq max(kr_0, 1) + 30$. An important factor is the influence of the discretization of the FEM part on the solution for $kr_0 < 1$. We consider the case of one, five and ten layers of elements to discretize the FEM part. This is important for low frequencies as the solution $H_0(kr)$ has a singularity when $k \to 0$. To improve the mesh, the FEM part discretizes the domain such that $kr_0 \leq kr \leq 1$ with thicknesses of layers in

geometric progression of step 0.7 in this domain. In figures 5(a) and (b), for a very low frequency such that $kr_0 = 1/1000$, we see that a mesh with three layers is sufficient to get very good results. When $kr_0 \geq 0.1$ only one layer is enough to obtain good results. So numerical solutions are very close to the analytical values with a simple mesh of the FEM part except for a very low value of kr_0 for which more element are needed in that domain to approach the singularity of the solution. For values of kr_0 larger than one, one sees in figure

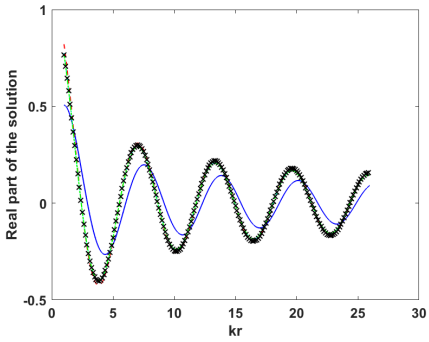

(a) $kr_0 = 1/1000, real\ part$

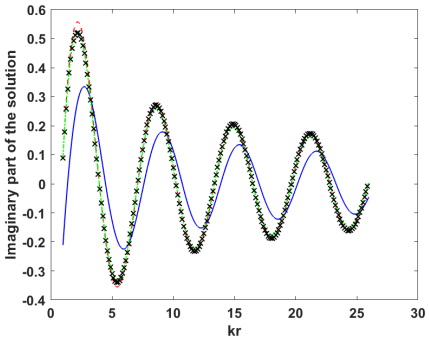

(b) $kr_0 = 1/1000, imaginary\ part$

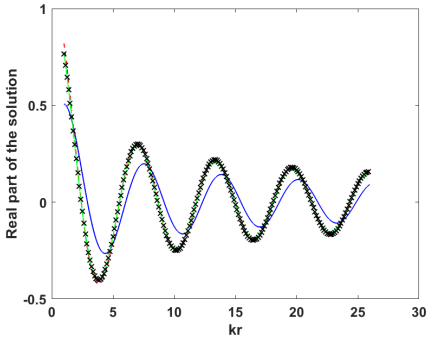

(c) $kr_0 = 1/100, real\ part$

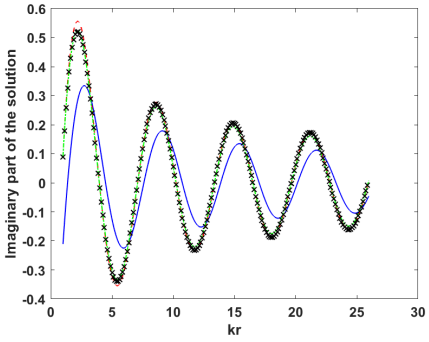

(d) $kr_0 = 1/100, imaginary\ part$

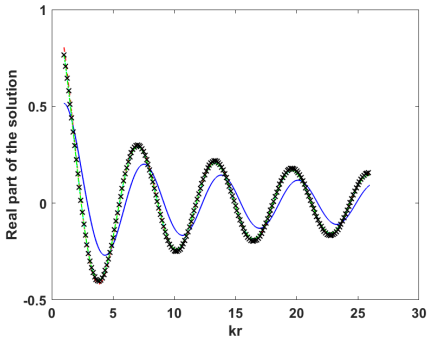

(e) $kr_0 = 1/10, real\ part$

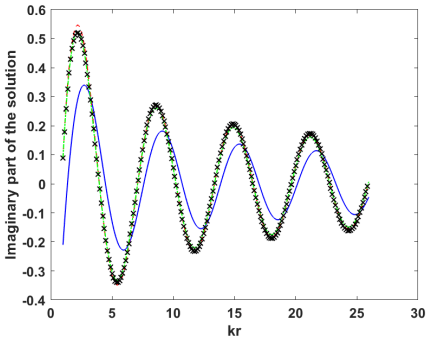

(f) $kr_0 = 1/10, imaginary\ part$

Fig. 6. Solutions for different values of kr_0 and nc (number of layers in the FEM part): — nc = 0, - - nc = 1,... nc = 3,-.- nc = 5, x analytical solution.

7 that the expansion is sufficient to get good results and it is not necessary to have a classical finite element mesh of a domain as for $kr_0 < 1$. One must also note that it is possible to get accurate results for a very large range of

values of kr_0 starting from very low frequencies at $kr_0 = 0.001$ to very high frequencies such that $kr_0 = 1000$.

3.2 Two-dimensional circular example

We consider now the radiation by a circle with a Dirichlet boundary condition and a solution satisfying the Helmholtz equation (1) in the exterior domain. To be able to compare with analytical solutions, the boundary value is first built from the field created by a source at a position $\mathbf{r}_s = (x_s, y_s)$ inside the circle. So the boundary value is

$$q_0(\mathbf{r}_b) = H_0(k|\mathbf{r}_b - \mathbf{r}_s|) \tag{39}$$

with $\mathbf{r}_b$ the position of a node on the boundary. We first study the influence of the parameter P giving the number of layers on the solution. In figure 8 we plot the L^2 relative error on the solution on the line $1m \leq x \leq 12m$ for the case of an axisymmetric solution obtained with $\mathbf{r}_s = (0, 0)$ and a non axisymmetric case obtained with $\mathbf{r}_s = (0.8m, 0m)$. In both cases, the boundary is the circle with $r_0 = 1m$, the frequency is $f = 1000Hz$ and the velocity is $340m/s$. Each layer is meshed first with linear four nodes elements, secondly with height nodes quadratic elements and the thickness is $e = 0.001m$. In all cases, the frequency is high enough so that no mesh of a FEM part is needed and only the expansion is used to build the solution. One can see that the optimal value of P is around 9 and that the error is reduced, as expected, by increasing the number of elements on the boundary. Taking second order elements clearly improves the solution for values of P around 9.

We now study the influence of the frequency and plot images of the solution on an annular domain. The source is at $(0.8m, 0m)$ and $kr_0 = 10$. We plot the solution between radius $r_0 = 1m$ and $7m$ in figure 9. One can observe a very good agreement between the numerical and analytical solutions.

We consider now the diffraction of a point source by a rigid cylinder of the same geometry. The source is located at $(-2m, 0)$. $P = 9$ and 500 elements are used upto $kr_0 = 10$ while 1000 elements and $P = 12$ are used for $kr_0 = 30$. The solution is plotted on a semi circle of radius $2m$ between the angle $-\pi$ and 0. Figure 10 presents the comparison between the present numerical solution and the analytical solution. Good agreement can be observed.

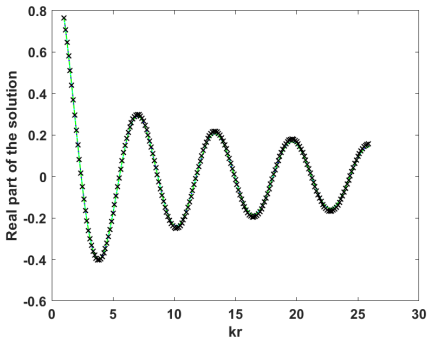

(a) $kr_0 = 1, real\ part$

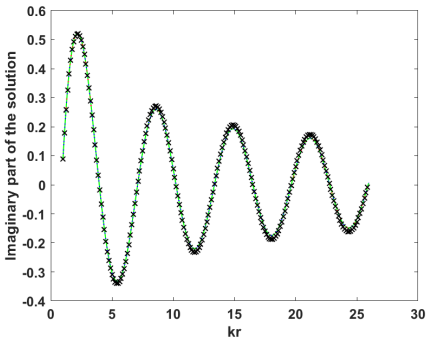

(b) $kr_0 = 1, imaginary\ part$

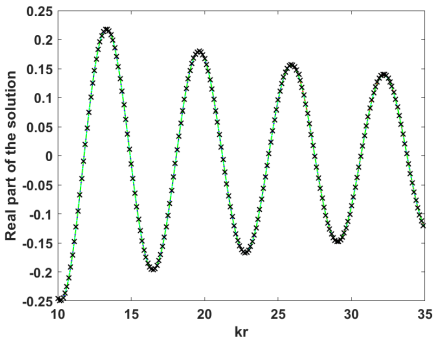

(c) $kr_0 = 10, real\ part$

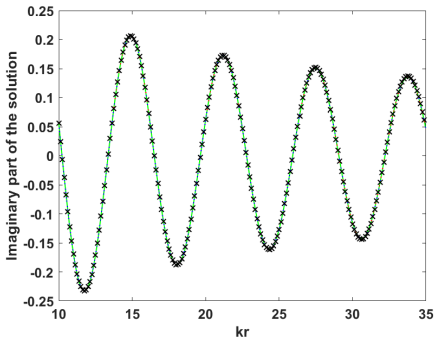

(d) $kr_0 = 10, imaginary\ part$

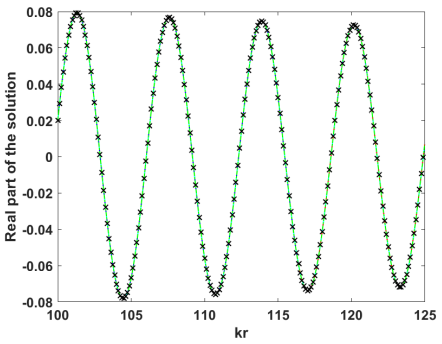

(e) $kr_0 = 100, real\ part$

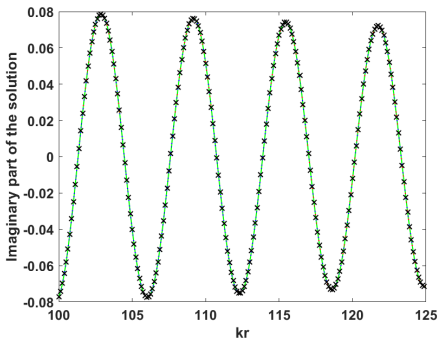

(f) $kr_0 = 100, imaginary\ part$

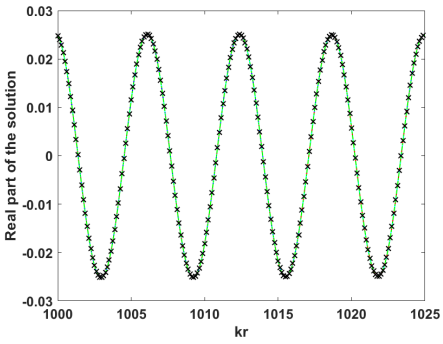

(g) $kr_0 = 1000, real\ part$

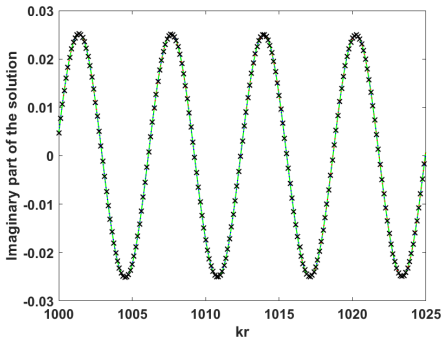

(h) $kr_0 = 1000, imaginary\ part$

Fig. 7. Solutions for different values of kr_0 and nc: — nc = 0, - - nc = 1,... nc = 3,-.- nc = 5, x analytical solution.

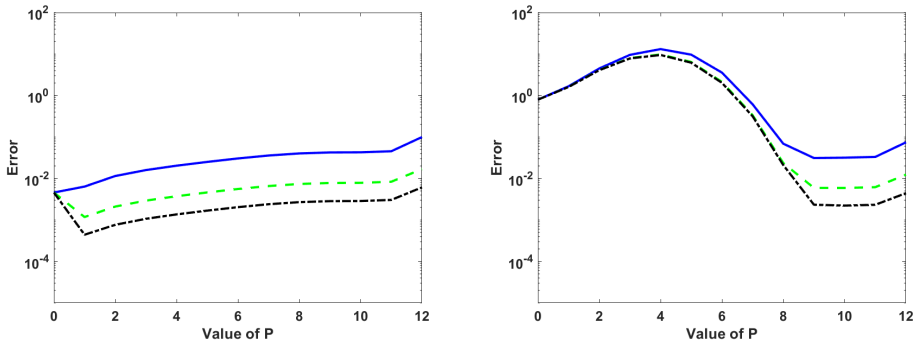

(a) axisymmetric and degree 1 (b) non symmetric and degree 1

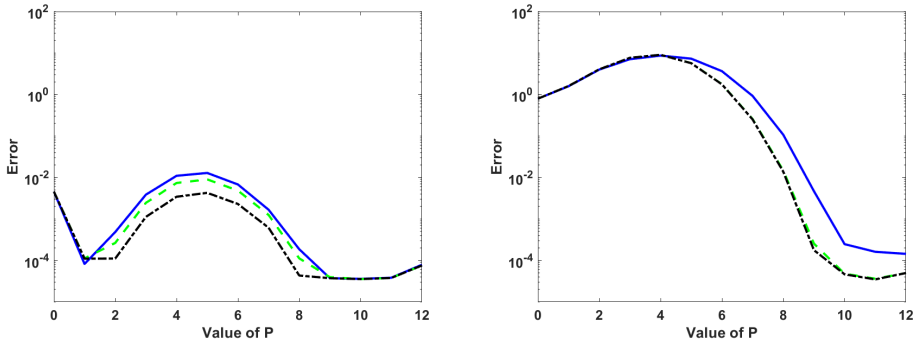

(c) axisymmetric and degree 2 (d) non symmetric and degree 2

Fig. 8. Error on the solution for different values of P and number of elements on the boundary, — 100 elements,- - 250 elements,-.- 500 elements.

3.3 Two-dimensional square example

We consider now the case of a square with a side of length $2m$ to test a domain with corners. As for the circle, a point source is located inside the square to build an analytical solution on the boundary. This source is located at $(0.5m, 0.5m)$. In figure 11, one compares the error for first and second order elements. One note a considerable improvement using elements of degree two.

Figure 12 presents the analytical and numerical solutions in the domain external to the square. The frequency is 500Hz, the elements are second order and each side is mesh with 200 elements. One can observe a very good agreement between the two solutions and that the corners do not create any particular problem.

3.4 Case of a resonant cavity

To finish, we consider the case of the circular and triangular resonant cavities presented on the left of figures 13 and 14. On the right of these figures, one

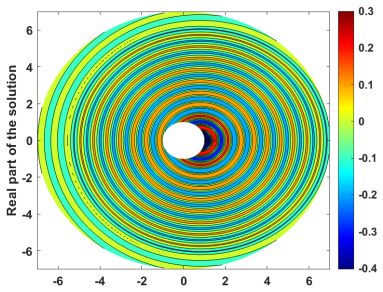

(a) Numerical solution, real part.

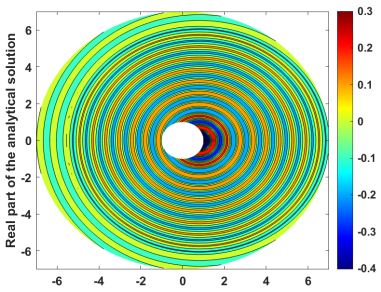

(b) Analytical solution, real part

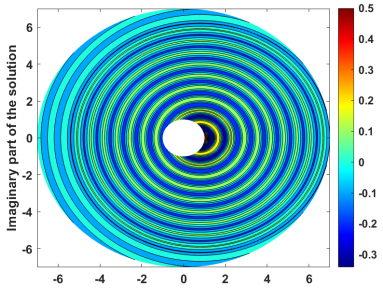

(c) Numerical solution, imaginary part.

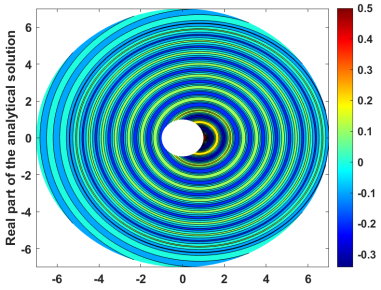

(d) Analytical solution, imaginary part.

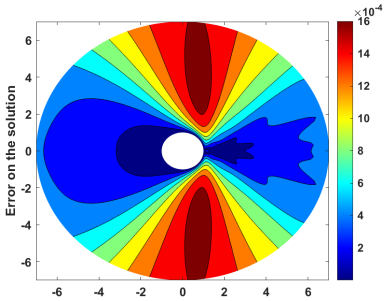

(e) Error on the solution.

Fig. 9. Numerical solution, analytical solution and error on an annular domain for $kr_0 = 10$.

has the meshes of the different exterior domains used for satisfying equations (24). A power four progression was found satisfactory such that in term of ξ we apply the relation on surfaces such that $\xi = 1 + d \times n^4$. For the circular resonator the interior radius is $0.06m$, the medium radius is $0.09m$ and the exterior radius which also defines the surface S_0 has a radius of $0.1m$. The opening connecting the interior cavity to the exterior domain has a width of $0.5cm$. For the triangular resonator, the vertex points of the triangles are located on the same circles as for the circular case and the opening connection has the same size. The mesh, stiffness and mass matrices were created with FEniCS and then imported into Matlab. Any other finite element software could have been used. In the case of the circular cavity, a sound source was put at point $(0.2m, 0)$ in front of the opening and the sound pressure was

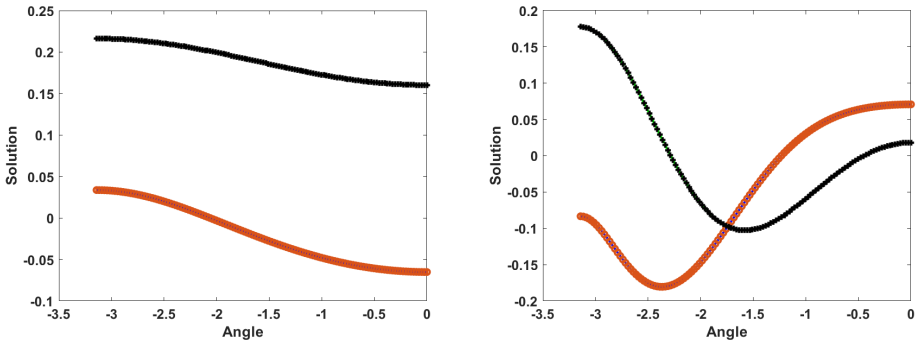

(a) $kr_0 = 0.1$ (b) $kr_0 = 1$

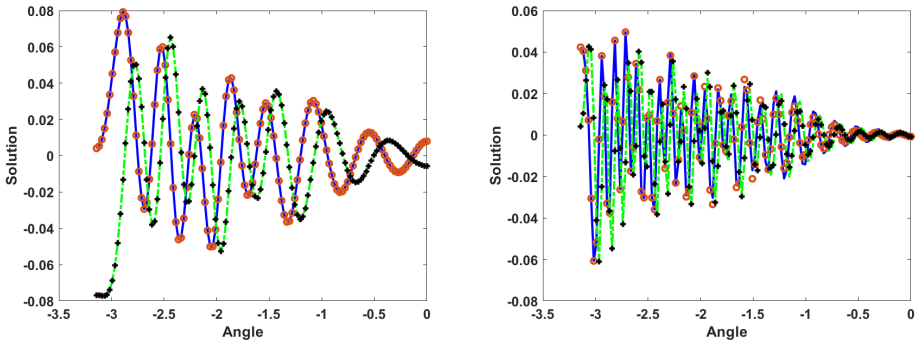

(c) $kr_0 = 10$ (d) $kr_0 = 30$

Fig. 10. Comparison of numerical and analytical solutions on a semi circle for different frequencies, — real part analytical, o real part numerical, -.- imaginary part analytical, + imaginary part numerical.

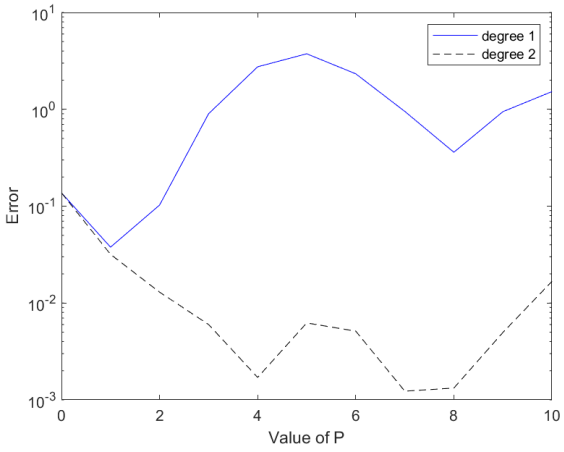

Fig. 11. Error for first (—) and second (- -) order elements in case of a square.

computed at the center of the cavity. The sound pressure versus the frequency is presented in figures 15a and 15b and compared to a BEM computation (obtained with a personal software of the author). A good agreement between the two solutions validates the accuracy of the present method. This can be observed both in term of modulus and real and imaginary parts. We see in

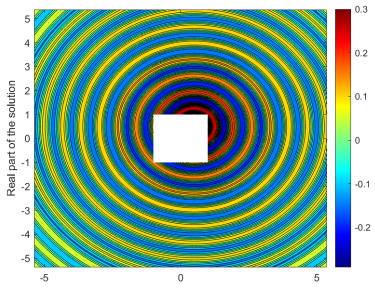

(a) Numerical solution, real part.

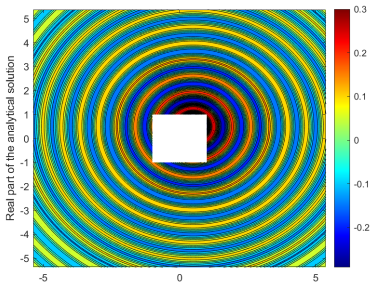

(b) Analytical solution, real part

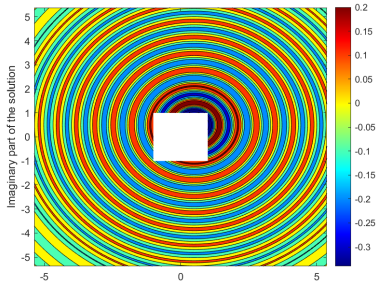

(c) Numerical solution, imaginary part.

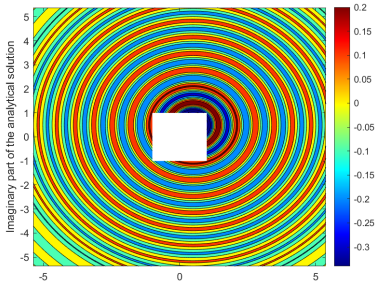

(d) Analytical solution, imaginary part.

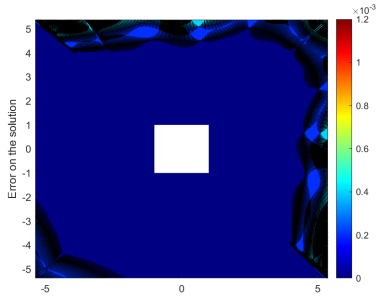

(e) Error on the solution.

Fig. 12. Numerical solution, analytical solution and error on a square domain for the frequency 500Hz.

particular that the resonance of the cavity is well reproduced.

Figures 16a and 16b consider the triangular resonator whose main difference is a non smooth geometry. The sound source is located at point $(0, -0.2m)$. In this case again the comparison between the BEM results and the present method is very good. Note that we see in figure 14 that only a small mesh in the exterior domain of the resonator is used because the scale domains follow the triangular geometry as can be seen in these figures.

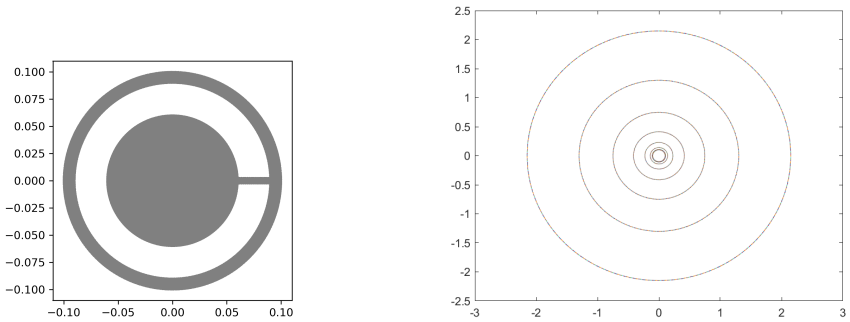

Fig. 13. Mesh of circular resonant cavity and its exterior domain.

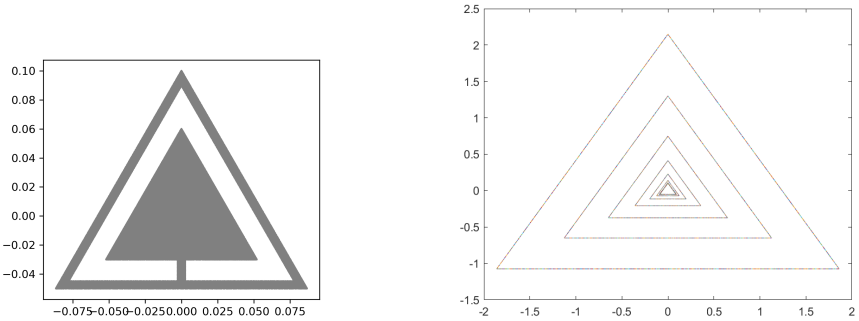

Fig. 14. Mesh of triangular resonant cavity and its exterior domain.

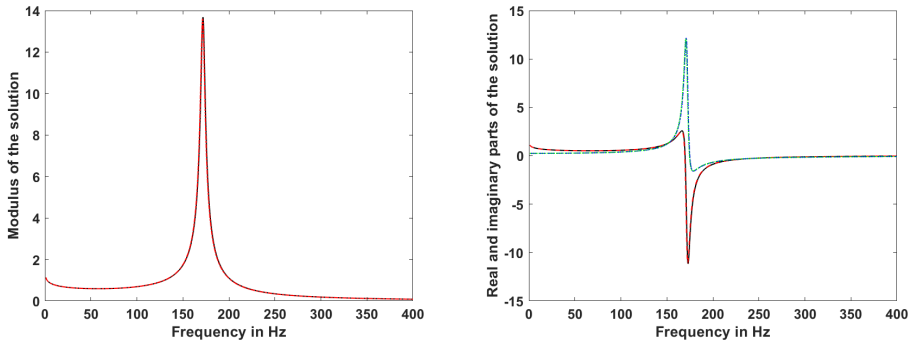

(a) Comparison between BEM (-.-) and the present method (—) for the modulus of the solution of the circular resonator.

(b) Comparison between BEM (- - real part, ... imaginary part) and the present method (— real part, -.- imaginary part).

Fig. 15. Results for the circular resonator.

4 Conclusion

A new numerical method has been presented for computing radiation and scattering of waves in exterior domains. The solution on the exterior domain is decomposed into the sum of products of polynomial and exponential functions

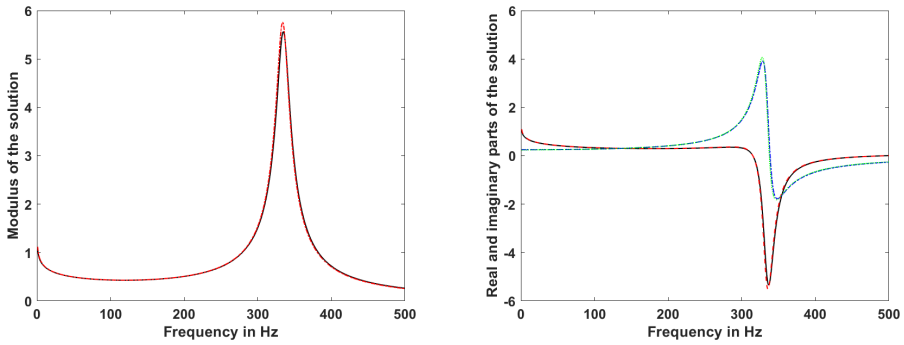

(a) Comparison between BEM (-.-) and the present method (—) for the modulus of the solution of the triangle resonator.

(b) Comparison between BEM (- - real part, ... imaginary part) and the present method (— real part, -.- imaginary part).

Fig. 16. Results for the triangular resonator.

multiplied by discrete FEM vectors. As in the scaled boundary element method there is no need of a fundamental solution but contrary to this method there is also no need of special matrices. The matrices involved in this problem are obtained from classical mass and stiffness matrices from any standard finite element software. One can note that the usual Scaled boundary finite element method (SBFEM) requires the solution of an eigenvalue problem while in the method proposed in this article, there are no modes to calculate but only the solution of a sparse linear system. For a large number of degree of freedom, this can certainly be more efficient. Examples show good agreements with analytical and BEM results. Future work should consider the optimisation of this method, the case of three-dimensional problems and other wave problems such as elastic wave propagation.

References

[1] C. A. Brebbia, S. Walker, Boundary Element Techniques in Engineering, Newnes-Butterworths, London, England, 1980.

[2] S. L. Crouch, A. M. Starfield, Boundary element methods in solid mechanics, Unwin Hyman, London, England, 1990.

[3] R. D. Ciskowski, C. A. Brebbia, Boundary Element Methods in Acoustics, Computational mechanics publications, Elsevier, Southampton, England, 1991.

[4] G. Chen, J. Zhou, Boundary element methods, Computational mathematics and applications, Academic press, London, 1992.

[5] M. Bonnet, Boundary Integral Equation Methods for Solids and Fluids, John Wiley and Sons, Chichester, England, 1995.

[6] V. Rokhlin, Rapid solution of integral equations of classical potential theory, Journal of Computational Physics 60 (2) (1985) 187–207.

[7] V. Rokhlin, Rapid solution of integral equations of scattering theory in two dimensions, Journal of Computational Physics 86 (2) (1990) 414–439.

[8] E. Darve, The fast multipole method: Numerical implementation, Journal of Computational Physics 160 (1) (2000) 195–240.

[9] Y. J. Liu, N. Nishimura, The fast multipole boundary element method for potential problems: A tutorial, Engineering Analysis with Boundary Elements 30 (5) (2006) 371–381.

[10] D. Givoli, J. B. Keller, A finite element method for large domains, Computer Methods in Applied Mechanics and Engineering 76 (1) (1989) 41–66.

[11] J. B. Keller, D. Givoli, Exact non-reflecting boundary conditions, Journal of computational physics 82 (1) (1989) 172–192.

[12] B. Engquist, A. Madja, Absorbing boundary conditions for the numerical simulation of waves, Math. Comp. 31 (139) (1977) 629–651.

[13] P. Bettess, Infinite elements, International Journal for Numerical Methods in Engineering 11 (1) (1977) 53–64.

[14] P. Bettess, More on infinite elements, International Journal for Numerical Methods in Engineering 15 (11) (1980) 1613–1626.

[15] P. Bettess, Infinite Elements, Penshaw Press, 1992.

[16] D. Burnett, A three-dimensional acoustic infinite element based on a prolate spheroidal multipole expansion, Journal of the Acoustical Society of America 96 (1994) 2798–2816.

[17] R. Astley, Infinite elements for wave problems: a review of current formulations and an assessment of accuracy, International Journal for Numerical Methods in Engineering 49 (7) (2000) 951–976.

[18] K. Gerdes, A review of infinite element methods for exterior helmholtz problems, Journal of Computational Acoustics 8 (01) (2000) 43–62.

[19] B. Engquist, A. Majda, Absorbing boundary conditions for numerical simulation of waves, Proceedings of the National Academy of Sciences 74 (5) (1977) 1765–1766.

[20] B. Engquist, A. Majda, Absorbing boundary conditions for numerical simulation of waves, Mathematics of Computation 31 (139) (1977) 629–651.

[21] R. Clayton, B. Engquist, Absorbing boundary conditions for acoustic and elastic wave equations, Bulletin of the Seismological Society of America 67 (6) (1977) 1529–1540.

[22] A. C. Reynolds, Boundary conditions for the numerical solution of wave propagation problems, Geophysics 43 (6) (1978) 1099–1110.

[23] A. Bayliss, E. Turkel, Radiation boundary conditions for wave-like equations, Communications on Pure and Applied Mathematics 33 (6) (1980) 707–725.

[24] A. Bayliss, M. Gunzburger, E. Turkel, Boundary conditions for the numerical solution of elliptic equations in exterior regions, SIAM Journal on Applied Mathematics 42 (2) (1982) 430–451.

[25] R. Higdon, Absorbing boundary conditions for difference approximations to the multidimensional wave equation, Mathematics of Computation 47 (176) (1986) 437–459.

[26] R. Higdon, Numerical absorbing boundary conditions for the wave equation, Mathematics of Computation 49 (179) (1987) 65–90.

[27] F. Collino, High-order absorbing boundary conditions for wave propagation models. straight line boundary and corner cases, in: Proc. 2nd Int. Conf. on Mathematical & Numerical Aspects of Wave Propagation, R. Kleinmanet al.SIAM, Delaware, USA, 1993, pp. 161–171.

[28] T. Hagstrom, S. Hariharan, A formulation of asymptotic and exact boundary conditions using local operators, Applied Numerical Mathematics 27 (4) (1998) 403 – 416.

[29] D. Givoli, High-order local non-reflecting boundary conditions: a review, Wave Motion 39 (4) (2004) 319–326.

[30] J. P. Berenger, A perfectly matched layer for the absorption of electromagnetic waves, Journal of computational physics 114 (2) (1994) 185–200.

[31] J. P. Berenger, Three-dimensional perfectly matched layer for the absorption of electromagnetic waves, Journal of computational physics 127 (2) (1996) 363–379.

[32] D. Duhamel, T. M. Nguyen, Finite element computation of absorbing boundary conditions for time-harmonic wave problems, Computer Methods in Applied Mechanics and Engineering 198 (37) (2009) 3006–3019.

[33] P. Bettess, Short-wave scattering: Problems and techniques, Philosophical transactions. Series A, Mathematical, physical, and engineering sciences 362 (2004) 421–443.

[34] C. Song, J. P. Wolf, Consistent infinitesimal finite-element cell method: three-dimensional vector wave equation, International Journal for Numerical Methods in Engineering 39 (13) (1996) 2189–2208.

[35] C. Song, J. P. Wolf, The scaled boundary finite-element method—alias consistent infinitesimal finite-element cell method—for elastodynamics, Computer Methods in Applied Mechanics and Engineering 147 (3) (1997) 329–355.

[36] C. Song, J. P. Wolf, The scaled boundary finite-element method: analytical solution in frequency domain, Computer Methods in Applied Mechanics and Engineering 164 (1) (1998) 249–264.

[37] J. P. Wolf, C. Song, Unit-impulse response of unbounded medium by scaled boundary finite-element method, Computer Methods in Applied Mechanics and Engineering 159 (3) (1998) 355–367.

[38] J. P. Wolf, C. Song, The scaled boundary finite-element method – a primer: derivations, Computers & Structures 78 (1) (2000) 191–210.

[39] C. Song, J. P. Wolf, The scaled boundary finite-element method – a primer: solution procedures, Computers & Structures 78 (1) (2000) 211–225.

[40] J. Wolf, C. Song, The scaled boundary finite-element method - a fundamental solution-less boundary-element method, Computer Methods in Applied Mechanics and Engineering 190 (2001) 5551–5568.

[41] C. Song, Dynamic analysis of unbounded domains by a reduced set of base functions, Computer Methods in Applied Mechanics and Engineering 195 (2006) 4075–4094.

[42] Z. J. Yang, A. J. Deeks, H. Hao, A Frobenius solution to the scaled boundary finite element equations in frequency domain for bounded media, International Journal for Numerical Methods in Engineering 70 (12) (2007) 1387–1408.

[43] C. Song, M. H. Bazyar, Development of a fundamental-solution-less boundary element method for exterior wave problems, Communications in Numerical Methods in Engineering 24 (4) (2008) 257–279.

[44] C. Birk, D. Chen, C. Song, C. Du, The scaled boundary finite element method for transient wave propagation problems, in: S. Klinkel, C. Butenweg, G. Lin, B. Holtschoppen (Eds.), Seismic Design of Industrial Facilities, Springer Fachmedien Wiesbaden, Wiesbaden, 2014, pp. 547–556.

[45] Z.-J. Yang, F. Yao, E.-T. Ooi, X.-W. Chen, A scaled boundary finite element formulation for dynamic elastoplastic analysis, International Journal for Numerical Methods in Engineering 120 (4) (2019) 517–536.

[46] H. Gravenkamp, C. Song, J. Zhang, On mass lumping and explicit dynamics in the scaled boundary finite element method, Computer Methods in Applied Mechanics and Engineering 370 (2020) 113274.

[47] N. Sepehry, M. Ehsani, W. Zhu, F. Bakhtiari-Nejad, Application of scaled boundary finite element method for vibration-based structural health monitoring of breathing cracks, Journal of Vibration and Control (2020). doi:10.1177/1077546320968646.

[48] L. Lehmann, S. Langer, D. Clasen, Scaled boundary finite element method for acoustics, Journal of Computational Acoustics 14 (04) (2006) 489–506.

[49] R. Nelson, S. Dong, R. Kalra, Vibrations and waves in laminated orthotropic circular cylinders, Journal of Sound and Vibration 18 (3) (1971) 429–444.

[50] B. Aalami, Waves in Prismatic Guides of Arbitrary Cross Section, Journal of Applied Mechanics 40 (4) (1973) 1067–1072.

[51] L. Gavrić, Computation of propagative waves in free rail using a finite element technique, Journal of Sound and Vibration 185 (3) (1995) 531–543.

[52] P. J. Shorter, Wave propagation and damping in linear viscoelastic laminates, The Journal of the Acoustical Society of America 115 (5) (2004) 1917–1925.

[53] I. Bartoli, A. Marzani, F. Lanza di Scalea, E. Viola, Modeling wave propagation in damped waveguides of arbitrary cross-section, Journal of Sound and Vibration 295 (3) (2006) 685–707.

[54] A. Marzani, E. Viola, I. Bartoli, F. Lanza di Scalea, P. Rizzo, A semi-analytical finite element formulation for modeling stress wave propagation in axisymmetric damped waveguides, Journal of Sound and Vibration 318 (3) (2008) 488–505.

[55] F. Treyssède, L. Laguerre, Investigation of elastic modes propagating in multi-wire helical waveguides, Journal of Sound and Vibration 329 (10) (2010) 1702–1716.

[56] K. Nguyen, F. Treyssède, C. Hazard, Numerical modeling of three-dimensional open elastic waveguides combining semi-analytical finite element and perfectly matched layer methods, Journal of Sound and Vibration 344 (2015) 158–178.

[57] W. Li, R. A. Dwight, T. Zhang, On the study of vibration of a supported railway rail using the semi-analytical finite element method, Journal of Sound and Vibration 345 (2015) 121–145.

[58] C. Hakoda, C. Lissenden, J. L. Rose, Weak form implementation of the semi-analytical finite element (SAFE) method for a variety of elastodynamic waveguides, AIP Conference Proceedings 1949 (1) (2018) 230001.

[59] C. Long, P. Loveday, D. Ramatlo, E. Andhavarapu, Numerical verification of an efficient coupled SAFE-3D FE analysis for guided wave ultrasound excitation, Finite Elements in Analysis and Design 149 (2018) 45–56.

[60] T. Khajah, L. Liu, C. Song, H. Gravenkamp, Shape optimization of acoustic devices using the scaled boundary finite element method, Wave Motion 104 (2021) 102732.

[61] B. Mace, D. Duhamel, M. Brennan, L. Hinke, Finite element prediction of wave motion in structural waveguides, Journal of the Acoustical Society of America 117 (2005) 2835–2843.

[62] D. Duhamel, B. R. Mace, M. J. Brennan, Finite element analysis of the vibrations of waveguides and periodic structures, Journal of Sound and Vibration 294 (1-2) (2006) 205–220.

[63] J.-M. Mencik, D. Duhamel, A wave-based model reduction technique for the description of the dynamic behavior of periodic structures involving arbitrary-shaped substructures and large-sized finite element models, Finite Elements in Analysis and Design 101 (2015) 1–14.

[64] J.-M. Mencik, M. N. Ichchou, Multi-mode propagation and diffusion in structures through finite elements, European Journal of Mechanics - A/Solids 24 (5) (2005) 877–898.

[65] J.-M. Mencik, D. Duhamel, A wave finite element-based approach for the modeling of periodic structures with local perturbations, Finite Elements in Analysis and Design 121 (2016) 40 – 51.

[66] J.-M. Mencik, New advances in the forced response computation of periodic structures using the wave finite element (WFE) method, Computational Mechanics 54 (3) (2014) 789–801.

[67] J.-M. Mencik, A model reduction strategy for computing the forced response of elastic waveguides using the wave finite element method, Computer Methods in Applied Mechanics and Engineering 229-232 (2012) 68–86.

[68] J.-M. Mencik, A wave finite element approach for the analysis of periodic structures with cyclic symmetry in dynamic substructuring, Journal of Sound and Vibration 431 (2018) 441–457.

[69] M. N. Ichchou, J.-M. Mencik, W. J. Zhou, Wave finite elements for low and mid-frequency description of coupled structures with damage, Computer Methods in Applied Mechanics and Engineering 198 (15-16) (2009) 1311–1326.

[70] T. Hoang, D. Duhamel, G. Foret, Wave finite element method for waveguides and periodic structures subjected to arbitrary loads, Finite Elements in Analysis and Design 179 (2020) 103437.

[71] J. M. Renno, B. R. Mace, On the forced response of waveguides using the wave and finite element method, Journal of Sound and Vibration 329 (26) (2010) 5474 – 5488.

[72] Y. Waki, B. Mace, M. Brennan, Free and forced vibrations of a tyre using a wave/finite element approach, Journal of Sound and Vibration 323 (3) (2009) 737 – 756.

[73] R. Singh, C. Droz, M. Ichchou, F. Franco, O. Bareille, S. De Rosa, Stochastic wave finite element quadratic formulation for periodic media: 1D and 2D, Mechanical Systems and Signal Processing 136 (2020) 106431.

[74] Y. Fan, C. Zhou, J. Laine, M. Ichchou, L. Li, Model reduction schemes for the wave and finite element method using the free modes of a unit cell, Computers & Structures 197 (2018) 42 – 57.

[75] A. Hvatov, S. Sorokin, On application of the Floquet theory for radially periodic membranes and plates, Journal of Sound and Vibration 414 (2018) 15–30.

[76] E. Manconi, S. Sorokin, R. Garziera, Wave propagation in polar periodic structures using Floquet theory and finite element analysis, in: 7th International Conference on Computational Methods in Structural Dynamics and Earthquake Engineering, Crete, Greece, 2019, pp. 3448–3456.